Evidence for an oscillatory singularity in generic $U(1)$ symmetric cosmologies on $T^3 \times R$

Beverly K. Berger *
Department of Physics, Oakland University, Rochester, MI 48309 USA

Vincent Moncrief †
Departments of Physics and Mathematics, Yale University, New Haven, CT 06520 USA

arXiv:gr-qc/9804085v1 30 Apr 1998

A longstanding conjecture by Belinskii, Lifshitz, and Khalatnikov that the singularity in generic gravitational collapse is locally oscillatory is tested numerically in vacuum, $U(1)$ symmetric cosmological spacetimes on $T^3 \times R$. If the velocity term dominated (VTD) solution to Einstein's equations is substituted into the Hamiltonian for the full Einstein evolution equations, one term is found to grow exponentially. This generates a prediction that oscillatory behavior involving this term and another (which the VTD solution causes to decay exponentially) should be observed in the approach to the singularity. Numerical simulations strongly support this prediction.

4.20.Dw, 98.80.Hw, 4.20.Cv, 95.30.Sf

I. INTRODUCTION

An important open question in classical general relativity is the nature of the singularities that form in generic gravitational collapse. The singularity theorems of Penrose [1], Hawking [2,3], and others [4,5] prove that some type of singular behavior must arise in generic gravitational collapse of reasonable matter. However, these theorems do not provide a description of the singular behavior that results. Many different types of singular behavior arise in known solutions to Einstein's equations. However, known explicit solutions tend to be characterized by simplifying symmetries. This means that singular behavior found in such examples need not be characteristic of those of generic collapse. In the 1960's, Belinskii, Khalatnikov, and Lifshitz (BKL) [6–10] claimed to have shown that, in the approach to the singularity, each spatial point of a generic solution behaves as a separate vacuum, Bianchi IX (Mixmaster [11]) homogeneous cosmology. Mixmaster cosmologies collapse as an infinite sequence of Bianchi I (Kasner [12]) spacetimes with a known relationship between one Kasner and the next [9,13]. Examinations of the BKL arguments [14] and attempts to provide a more rigorous basis for their claims [15] have until recently yielded little evidence one way or the other for their validity.

In the past decade, work has begun aimed at understanding the singularity and the approach to it in spatially inhomogeneous cosmologies [16–18]. If Einstein's equations are truncated by ignoring all terms with spatial derivatives and keeping all terms with time derivatives (for some more or less natural choice of spacetime slicing), the velocity term dominated (VTD) solutions are found. If an inhomogeneous spacetime is asymptotically VTD (AVTD), the evolution toward the singularity at (almost) every spatial point comes arbitrarily close to one of the VTD solutions [16,19]. It has been proven that polarized Gowdy cosmologies [20,21] and more general polarized T^2-symmetric models [22] are AVTD [16,23]. The main extra feature in generic Gowdy models compared to polarized ones is the presence of two nonlinear terms in the Hamiltonian which yields the dynamical Einstein equations. In an AVTD spacetime, these must become exponentially small as the singularity is approached. But this requirement is only consistent with the form of the VTD solution if a spatially dependent parameter of the VTD solution lies in a restricted range at (almost) every spatial point. The numerical studies demonstrate that the nonlinear terms act as potentials to drive the parameter into the consistent range [24]. Very recently, it has been proven that generic Gowdy solutions with a consistent value of this parameter are AVTD [25].

Recently, Weaver et al [26] have extended the Gowdy model by inclusion of a magnetic field (and change of spatial topology from T^3 to the solv-twisted torus [27]). This model is an inhomogeneous generalization of the magnetic Bianchi VI_0 homogeneous cosmology which is known to exhibit Mixmaster behavior [28,29]. The magnetic field causes a third nonlinear term to be present. This term grows for precisely that range of VTD parameter which makes the original two vacuum Gowdy nonlinear terms exponentially small. This prediction of local Mixmaster

*e-mail address: berger@oakland.edu
†e-mail address: moncrief@hepvms.physics.yale.edu

oscillations is observed in numerical simulations of the full Einstein equations. This study provided the first support in inhomogeneous cosmologies for the BKL claim.

To further explore this issue, we have generalized to the study of vacuum spacetimes on $T^3 \times R$ with one spatial $U(1)$ symmetry [30]. While such models are, of course, not generic solutions to Einstein's equations, they are considerably more complex than any previously considered for this purpose. Application of the methods previously described for Gowdy models leads to the predictions that (1) *polarized* $U(1)$ symmetric cosmologies should be AVTD [31] and (2) generic $U(1)$ models should have an oscillatory singularity. Numerical simulations have previously provided strong support for the predicted AVTD singularity in polarized $U(1)$ models [32]. Here we shall discuss the support we have obtained for the local oscillatory nature of the singularity in generic $U(1)$ models.

Unlike all previous cases discussed in this program [18,24,26,32], numerical difficulties require an introduction of spatial averaging (data smoothing) at each time step to prevent numerical instability. This averaging destroys convergence of the solution with increasing spatial resolution (see [33]). The need for spatial averaging can be traced to the growth of spiky features first seen and discussed in the Gowdy models [18,24]. These features also (as the bounces in Mixmaster itself [34]) make it necessary to explicitly enforce the Hamiltonian constraint. If this is not done, qualitatively incorrect behavior will result. We shall argue in this paper that, despite the need for spatial averaging and our simple algebraic method of enforcement of only the Hamiltonian constraint, the qualitative behavior of the numerical simulations is correct. We believe we have demonstrated that the singularity in generic $U(1)$ symmetric cosmologies is spacelike, local, and oscillatory. Evidence for this is that the oscillations and their correlation with the exponential growth of certain nonlinear terms in Einstein's equations are independent of spatial resolution and choice of initial data.

A brief review of generic $U(1)$ models, their VTD solution, and the prediction of oscillatory behavior are given in Section II. In Section III we describe the numerical issues and results. Discussion is given in Section IV.

II. THE MODEL

As discussed in more detail elsewhere [32], $U(1)$ symmetric cosmologies on $T^3 \times R$ are described by the metric

$$ds^2 = e^{-2\varphi}\left\{-e^{2\Lambda}e^{-4\tau}d\tau^2 + e^{-2\tau}e^{\Lambda}e_{ab}dx^a dx^b\right\} + e^{2\varphi}\left(dx^3 + \beta_a dx^a\right)^2 \tag{1}$$

where φ, β_a, z, x, Λ are functions of spatial variables u, v and time τ, sums are over a, $b = u$, v, and

$$e_{ab} = \tfrac{1}{2}\begin{bmatrix} e^{2z} + e^{-2z}(1+x)^2 & e^{2z} + e^{-2z}(x^2-1) \\ e^{2z} + e^{-2z}(x^2-1) & e^{2z} + e^{-2z}(1-x)^2 \end{bmatrix} \tag{2}$$

is the conformal metric of the u-v plane. A canonical transformation replaces the twists β_a and their conjugate momenta e^a with the twist potential ω and its conjugate momentum r [30,32]. The dynamical variables φ and ω are respectively related to the amplitude for the + and × polarizations of gravitational waves and propagate in a background spacetime described by z, x, and Λ. Our coordinate choice ($N = e^{\Lambda}$, zero shift) does not significantly restrict the generality of these models [30]. Einstein's evolution equations (in vacuum) are found from the variation of [32]

$$\begin{aligned} H &= \int\int du\,dv\,\mathcal{H} \\ &= \int\int du\,dv\left(\tfrac{1}{8}p_z^2 + \tfrac{1}{2}e^{4z}p_x^2 + \tfrac{1}{8}p^2 + \tfrac{1}{2}e^{4\varphi}r^2 - \tfrac{1}{2}p_\Lambda^2 + 2p_\Lambda\right) \\ &\quad + e^{-2\tau}\int\int du\,dv\left\{\left(e^{\Lambda}e^{ab}\right)_{,ab} - \left(e^{\Lambda}e^{ab}\right)_{,a}\Lambda_{,b} + e^{\Lambda}\left[\left(e^{-2z}\right)_{,u}x_{,v} - \left(e^{-2z}\right)_{,v}x_{,u}\right]\right. \\ &\quad \left. + 2e^{\Lambda}e^{ab}\varphi_{,a}\varphi_{,b} + \frac{1}{2}e^{\Lambda}e^{-4\varphi}e^{ab}\omega_{,a}\omega_{,b}\right\} \\ &= H_K + H_V = \int\int du\,dv\,\mathcal{H}_K + \int\int du\,dv\,\mathcal{H}_V \end{aligned} \tag{3}$$

where $\{p, r, p_x, p_z, p_\Lambda\}$ are respectively canonically conjugate to $\{\varphi, \omega, x, z, \Lambda\}$. The constraints are

$$\mathcal{H}^0 = \mathcal{H} - 2p_\Lambda = 0 \tag{4}$$

and

$$\mathcal{H}_u = p_z\, z_{,u} + p_x\, x_{,u} + p_\Lambda\, \Lambda_{,u} - p_{\Lambda,u} + p\varphi_{,u} + r\omega_{,u} + \tfrac{1}{2}\left\{\left[e^{4z} - (1+x)^2\right] p_x - (1+x)p_z\right\}_{,v}$$
$$-\tfrac{1}{2}\left\{\left[e^{4z} + (1-x^2)\right] p_x - x p_z\right\}_{,u} = 0, \tag{5}$$

$$\mathcal{H}_v = p_z\, z_{,v} + p_x\, x_{,v} + p_\Lambda\, \Lambda_{,v} - p_{\Lambda,v} + p\varphi_{,v} + r\omega_{,v} - \tfrac{1}{2}\left\{\left[e^{4z} - (1-x)^2\right] p_x + (1-x)p_z\right\}_{,u}$$
$$+\tfrac{1}{2}\left\{\left[e^{4z} + (1-x^2)\right] p_x - x p_z\right\}_{,v} = 0. \tag{6}$$

The VTD solution has been given elsewhere [32]. Here we shall consider only the limit as $\tau \to \infty$ of this solution. (Recall that the VTD solution is found by eliminating all terms with spatial derivatives from Einstein's equations.) The limiting VTD solution is

$$z = -v_z\tau, \quad , x = x_0, \quad p_z = -4v_z, \quad p_x = p_x^0, \quad \varphi = -v_\varphi\tau,$$
$$\omega = \omega_0, \quad p = -4v_\varphi, \quad r = r^0, \quad \Lambda = \Lambda_0 + (2 - v_\Lambda)\tau, \quad p_\Lambda = v_\Lambda \tag{7}$$

where v_z, v_φ, x_0, p_x^0, ω_0, r^0, Λ_0, and $v_\Lambda > 0$ are functions of u and v but independent of τ. (The sign of v_Λ is fixed to ensure collapse.)

We now use the method of consistent potentials (MCP) [17] to determine the consistency of the VTD solution with the full Einstein equations. As $\tau \to \infty$, consistency requires that all terms other than those which yield (7) should become exponentially small. Rather than consider the equations, we shall examine the Hamiltonian density which generates them. Possible inconsistencies could arise from the nonlinear terms in (3) containing exponential factors. These same exponentials would, of course, be present in Einstein's equations. We first notice that the Gowdy-like terms [18]

$$V_z = \tfrac{1}{2}\, p_x^2\, e^{4z}, \quad V_1 = \tfrac{1}{2}\, r^2\, e^{4\varphi} \tag{8}$$

in $\mathcal{H}_K$ become, in the limit of $\tau \to \infty$, upon substitution of (7)

$$V_z \to \tfrac{1}{2}\, p_x^2\, e^{-4v_z\tau}, \quad V_1 \to \tfrac{1}{2}\, r^2\, e^{-4v_\varphi\tau} \tag{9}$$

and are exponentially small only if $v_z > 0$ and $v_\varphi > 0$. (As in the Gowdy case [24], non-generic behavior can arise at isolated spatial points where p_x and/or r vanish.)

The complicated terms in H containing the spatial derivatives have only two types of exponential behavior. All but one of the terms in $\mathcal{H}_V$ have a factor

$$e^{(-2\tau + \Lambda - 2z)} \tag{10}$$

(if we assume $v_z > 0$, all components of e_{ab} are dominated by e^{-2z}) which becomes

$$\approx e^{(-v_\Lambda + 2v_z)\tau} \tag{11}$$

in the VTD limit. The remaining term is

$$V_2 = \tfrac{1}{2} e^{-2\tau + \Lambda} e^{-4\varphi} e^{ab} \omega_{,a}\, \omega_b \tag{12}$$

which becomes upon substitution of (7)

$$V_2 \approx F(x, \nabla\omega) e^{(-v_\Lambda + 2v_z + 4v_\varphi)\tau} \tag{13}$$

where F is some function. The coefficients of τ in (11) and (13) are restricted by the VTD form of the Hamiltonian constraint (as $\tau \to \infty$)

$$\mathcal{H}^0 \approx -\tfrac{1}{2} v_\Lambda^2 + 2v_z^2 + 2v_\varphi^2 \approx 0 \tag{14}$$

obtained by substitution of (7) into (4). As discussed in [32], (14) implies that $v_\Lambda > 2v_z$ so that (11) decays exponentially for $v_z > 0$ for any v_φ. On the other hand, for V_2 to become exponentially small with v_z and $v_\varphi > 0$, we require $v_\Lambda^2 > (2v_z + 4v_\varphi)^2$ which is inconsistent with (14). Since there is no way to make V_1 and V_2 both exponentially small with the same value of v_φ, the MCP predicts that either V_1 or V_2 will always grow exponentially. (Again, non-generic behavior can result at isolated spatial points where the coefficient of V_2 happens to vanish.)

To refine this prediction, consider $v_z >> |v_\varphi|$. Substitution in (14) yields

$$v_\Lambda \approx 2v_z + \frac{v_\varphi^2}{v_z} \tag{15}$$

which shows that

$$V_2 \approx e^{4v_\varphi \tau} F(x, \nabla\omega) \quad , \quad V_1 \approx r^2 e^{-4v_\varphi \tau}. \tag{16}$$

Thus we expect V_1 and V_2 to act as potentials for the φ degree of freedom with a bounce off either potential causing the sign of v_φ to change. The remaining variables will follow the VTD solution with parameters which change at every bounce in φ. Thus we predict that oscillations in the φ degree of freedom will occur at (almost) every spatial point with different values of v_φ and coefficients of V_1 and V_2.

Note that in polarized $U(1)$ models, $\omega = r = 0$ so that the oscillations of (16) should be absent. Polarized $U(1)$ models should thus be AVTD. This is precisely what has been found in numerical simulations of these models [32].

III. RESULTS AND NUMERICAL ISSUES

In order to test the predictions of the previous section, we performed numerical simulations of the Einstein evolution equations obtained from the variation of (3). We use a symplectic PDE solver which has been described in great detail elsewhere [18,32,35–39]. In our previous study of polarized $U(1)$ models, we demonstrated convergence of the solutions at the expected order with increasing spatial resolution. Unfortunately, the re-introduction of the ω degree of freedom leads to the growth of spiky features absent in the polarized case. The origin of the spiky features is discussed elsewhere [24] but is related to the non-generic behavior at isolated spatial points. The spiky features which our methods easily treat in one spatial dimension [18] cannot be modeled sufficiently well in two spatial dimensions to prevent numerical instability. However, these instabilities can be suppressed in two ways. First, the simulations are begun at $\tau \approx 10$ or so to reduce the influence of $\mathcal{H}_V$ from (3). (This has the disadvantage, as in homogeneous Mixmaster spacetimes [40], of increasing the time interval between bounces.) Second, at every time step, all ten variables are replaced by their spatial "average." Any function $f(u, v)$ is replaced by [39]

$$\begin{aligned}\bar{f}(u,v) = c_0 f(u,v) + \sum_{i=1}^{5} c_i \, [&f(u + i\Delta u, v) + f(u, v + i\Delta v) \\ &+ f(u - i\Delta u, v) + f(u, v - i\Delta v) - 4f(u,v)]\end{aligned} \tag{17}$$

where $c_0 = 1/2$, $c_1 = 4867/38400$, $c_2 = -1067/28800$, $c_3 = -1237/691200$, $c_4 = 787/345600$, $c_5 = 31/691200$ and Δu, Δv are the grid spacings. This scheme is 6th order accurate (i.e. the difference between $\bar{f}(u, v)$ and $f(u, v)$ is 7th order in the grid spacings—actually 8th order due to symmetry). Where $f(u, v)$ is smooth, the averaging has no effect. However, it does spread out grid scale size spiky features. Unfortunately, the averaging process destroys the convergence seen in the polarized case (by examination of the deviation of the Hamiltonian and momentum constraints from zero [33]), as can be determined by adding averaging to polarized $U(1)$ simulations. We shall argue later that despite the absence of convergence in this sense, the qualitative behavior is still independent of spatial resolution. We shall further argue that the correct qualitative behavior is sufficent to determine the nature of the singularity in generic $U(1)$ models.

In Section II, we showed that the behavior of the potentials in $\mathcal{H}_V$ was restricted by the VTD limit of the Hamiltonian constraint (14). This means that it is essential to preserve the Hamiltonian constraint during the simulation. Failure to preserve $\mathcal{H}^0 = 0$ means that p_Λ would have the *wrong* dependence on p_z and p. This could change the sign of the coefficient of τ in (13). While solving the constraints initially is sufficient analytically, there is no way to guarantee that the differenced form of the constraints is preserved during a numerical simulation of the Einstein evolution equations. While in the polarized $U(1)$ case, the constraints can be seen to converge to zero [32], this is no longer true in generic $U(1)$ simulations with spatial averaging. To preserve the correct relationships among v_Λ, v_z, and v_φ from (14), we therefore solve $\mathcal{H}^0 = 0$ (4) for $p_\Lambda > 0$ algebraically at each time step. We note that this is the precise analog of the procedure used in Mixmaster itself [34]. However, spatial averaging must be performed on this new p_Λ which then yields a (small) non-zero value for $\mathcal{H}^0$. If we assume that $p_\Lambda = p_\Lambda^{\text{true}} + \Delta$ is the measured value, then (14) can be linearized in the error Δ and solved to yield

$$\Delta = -\frac{\mathcal{H}^0}{p_\Lambda} \tag{18}$$

where $\mathcal{H}^0$ is the measured, erroneous value of the Hamiltonian constraint. Substitution in $\alpha = -v_\Lambda + 2v_z + 4v_\varphi$, the coefficient of τ in V_2, yields a measured and true value for α. If the product $\alpha\,\alpha^{\text{true}}$ is positive everywhere for all τ,

the errors due to averaging cannot have changed the qualitative behavior since that just depends on the sign of α. Examination of the simulation data shows $\alpha\,\alpha^{\rm true} > 0$ at (almost) all spacetime points. Occasionally, early in the simulation, a few isolated points—in space and time—will show a sign change due to this error.

The momentum constraints (5) and (6) are freely evolved and do not remain especially small. However, they contain only spatial derivatives. Errors in the momentum constraints would therefore generate errors in the spatial dependence of the variables at a given time but not in their qualitative time dependence at each spatial point. A measure of the constraint convergence vs τ is shown in Figure 1. The freely evolved $\mathcal{H}_u$ ($\mathcal{H}_v \approx \mathcal{H}_u$) is actually larger at finer spatial resolution. This may be attributed to the larger spatial gradients observed at finer spatial resolution [24]. On the other hand, the error in the Hamiltonian constraint is converging to zero.

The restricted initial value solution for generic $U(1)$ models has been described elsewhere [32]. To solve the momentum constraints, we set $p_z = p_x = \varphi_{,a} = \omega_{,a} = 0$ and $p_\Lambda = ce^\Lambda$. For $c > 0$ sufficiently large, this allows the Hamiltonian constraint to be solved algebraically for p (case A) or r (case B). Four functions, x, z, Λ, and r (case A) or p (case B), may be freely specified. The detailed values used in the numerical simulations are given in the figure captions. While we shall present results for only two sets of initial data, the results are typical of all initial data and may be regarded to be characteristic of generic initial data.

Figures 2-4 show the behavior of φ, V_1, and V_2 for three spatial resolutions for case A initial data. In all cases, the behavior is exactly as predicted in Section II. Figure 5 shows a typical evolution for case B initial data, again showing the predicted behavior. For the simulation of Figure 3, the remaining variables ω, z, x, and Λ vs τ are shown at the same spatial point in Figure 6. Here we see approximate VTD behavior in ω, z, and Λ with parameters changing at the times of the φ bounces. While the behavior of x does not appear to be as predicted, we note from (7), (10), and (12) that only the behaviors of z and Λ are important to the local dynamics since only they appear in the arguments of exponentials. Finally, we display "movie frames" of $\mathcal{H}_V(u,v)$ and $\varphi(u,v)$ vs τ in Figures 7 and 8. Since $\mathcal{H}_V$ is shown on a logarithmic scale and φ on a linear one, Figure 7 is dominated by V_2 while Figure 8 indicates the behavior on a logarithmic scale of V_1. The predicted behavior that either V_1 or V_2 but not both be large is clearly seen in Figures 7 and 8. The bounces in φ occur at different spatial points at different times. This eventually will lead to increasingly complex spatial structure [41].

IV. DISCUSSION

Numerical simulations of generic $U(1)$ models demonstrate that the evolution toward the singularity is local and oscillatory due to the alternate expoential growth and decay of V_1 and V_2. This behavior requires that the time dependence of the coefficients of V_1 and V_2 and the coefficients of τ in the approximate forms of V_1 and V_2 be negligible (i.e. act on a much slower time scale) compared to the exponential time dependence obtained from the VTD solution. The qualitative behavior seen in the simulations indicates that this requirement is met (almost) everywhere sufficiently close to the singularity. Exceptional behavior at isolated spatial points similar to that found in simpler models [24,26] cannot be studied with the current numerical code. Exceptional behavior arises at isolated spatial points because one of the exponential potentials which causes the generic behavior is absent. While we believe we have identified the correct exponential behavior, the data we have on spatial dependence at a given time is probably not sufficiently reliable for conclusions about "higher order" effects.

The explanation for the local nature of the evolution is easy to obtain. From the metric (1), we see that the distance Δl traveled by a light ray away from the singularity from $\tau = \infty$ to $\tau = \tau_0$ (coordinate horizon size) is

$$\Delta l \approx \int_\infty^{\tau_0} e^{\Lambda/2+z-\tau} d\tau \tag{19}$$

where the VTD limit of e_{ab} has been used. Simulations demonstrate that the VTD solution may be used in (19) to give $\Delta l \to 0$ for the coordinate horizon size [21] as $\tau_0 \to \infty$. Since the horizon size is decreasing, the spatial points are unable to communicate with each other. But such communication occurs through changing spatial derivatives. If no communication can occur, the spatial derivative containing terms must be dynamically unimportant.

The primary question then is the extent to which the numerical results presented here are believable as evidence for the oscillatory nature of the singularity. It is easy to show, e.g. by comparing polarized $U(1)$ simulations with and without spatial averaging, that spatial averaging ruins convergence tests. Furthermore, non-zero values of the momentum constraints (5) and (6) indicate the presence of errors in the variables and their spatial derivatives. (Since rescaling the coordinates by a constant yields rescaled values of the constraints without changing the behavior of the solutions, one cannot attach any significance to the actual magnitude of the constraint violation.) Both sources of error—spatial averaging and constraint violation—principally affect details of the spatial dependence of the variables at a given time. Comparison of simulations at different spatial resolutions (and with quite different initial data) shows

that the qualitative time dependence at fixed spatial points is not affected by these errors. This is shown in Figure 9 where φ is shown on a line $u = v$ with $u, v \in [0, \pi]$ vs τ for three different spatial resolutions. While the features appear narrower at finer spatial resolution (see [24] for a similar phenomenon in Gowdy models), the time development of the simulations is remarkably consistent and independent of resolution. Figure 10 shows the final time step for φ for two different spatial resolutions. While the spatial dependence is quantitatively different, it is qualitatively quite similar. We also see in Figures 11 and 12, that the correlation between V_1 and V_2 seen at single spatial points in Figures 2-6 occurs everywhere. Figure 11 shows $\log_{10} V_1$ and $\log_{10} V_2$ on the line $u = v$ with $u, v \in [0, 2\pi]$ vs τ. Clearly, one potential grows as the other decays at all spatial points. Figure 12 shows the final time step for V_1, V_2, and φ on the line $u = v$ with $u, v \in [0, \pi]$. Given this same oscillatory behavior in all the simulations and the explanation for it in terms of the VTD solution given in Section II, it is proabable that we have correctly described the nature of the generic singularity in this class of models.

This does not mean that it is unimportant to improve the numerical treatment. Better numerics will yield more accurate spatial dependence of the metric variables. We expect to see ever narrowing spatial structure as in Gowdy [24] and magnetic Gowdy [26] models caused by non-generic values at isolated spatial points. This can also yield precise data for analysis of the local dynamics to characterize the "higher order" effects due to spatial inhomogeneity. It might also become possible to observe and characterize any other exceptional behavior that might arise at isolated spatial points.

There are several possibilities for numerical improvement. First among these is to incorporate into the algorithm the fact that a known explicit solution exists for the bounce (scattering) off an exponential potential. The symplectic algorithm divides the Hamiltonian for a system into two or more subhamiltonians with explicit exact solutions for their equations of motion. The standard division of H is into kinetic (H_K) and potential (H_V) pieces. Including a dominant exponential wall from H_V in H_K has yielded tens of orders of magnitude of improvement in speed while maintaining machine level precision in the ODE'S of spatially homogeneous Mixmaster models [34]. The current $U(1)$ code uses $\mathcal{H}_K$ and $\mathcal{H}_V$ (3) as the subhamiltonians. However, one could treat

$$\mathcal{H}_\varphi^{(1)} = \tfrac{1}{8}\, p^2 + \tfrac{1}{2} e^{\Lambda} e^{ab} e^{4\varphi} \omega_{,a}\, \omega_{,b} \tag{20}$$

or

$$\mathcal{H}_\varphi^{(2)} = \tfrac{1}{8}\, p^2 + \tfrac{1}{2} r^2\, e^{4\varphi} \tag{21}$$

as a separate subhamiltonian depending on which of V_1, V_2 is the larger. The absence of p_Λ, p_z, and r from (20) means that the equations from $\mathcal{H}_\varphi^{(1)}$ are exactly solvable (as, obviously are those from $\mathcal{H}_\varphi^{(2)}$). While in the ODE case, the main advantage was found in the ability to take huge time steps, for the $U(1)$ case, it will be the improved accuracy of the bounce solution. Another area of improvement is in spatial differencing. The current code uses 4th and 6th order accurate representations of first and second derivatives due to Norton [39]. These are designed to minimize the growth of grid scale wavelength instabilities. However, when applied to the Gowdy model, this scheme appears to be less stable than the original one [18] based on variation of a differenced form of the Hamiltonian. We also note that spectral methods have been tried but have not proven to be useful. A third place for numerical improvement would be to solve all three constraints rather than just the Hamiltonian constraint. Of course, one naturally wonders if adaptive mesh refinement (AMR) might yield improvements in accuracy and stability. Studies to date have shown that increasing spatial resolution yields only small improvements in stability. This is probably due to the fact that finer resolution only gives better representation of spiky features—showing them to be narrower and steeper than they appear at coarser resolution. In the Gowdy simulations, however, it was noticed that, for any given simulation, there is a threshold spatial resolution. If the resolution is coarser than that, the code will blow up before the AVTD regime is reached everywhere. It is therefore possible that we have not yet reached this threshold in the $U(1)$ case and thus would be helped by AMR. However, in the generic $U(1)$ models, there is no AVTD regime. Thus it is not clear if any spatial resolution could yield a simulation which could run indefinitely without crashing.

As a final note, we remark that the local nature of the $U(1)$ evolution (as well as the other cases we have studied) has two major implications:

(1) The use of cosmological boundary conditions is merely a convenience since they do not affect the local behavior. Any collapse of a system with one spatial Killing field to a spacelike singularity should be local and oscillatory.

(2) Qualitative answers on the nature of the singularity do not require fine spatial resolutions. This means that the zero Killing field case should be tractable numerically. Work on this case is in progress.

ACKNOWLEDGEMENTS

We would like to thank the Albert Einstein Institute at Potsdam for hospitality. BKB would also like to thank the Institute for Geophysics and Planetary Physics of Lawrence Livermore National Laboratory for hospitality. This work was supported in part by National Science Foundation Grants PHY9507313 and PHY9503133. Numerical simulations were performed at the National Center for Supercomputing Applications (University of Illinois).

FIGURE CAPTIONS

Figure 1. Convergence testing of constraints. The average values of the momentum constraint $\mathcal{H}_u$ (broken line) and Hamiltonian constraint $\mathcal{H}^0$ (solid line) are displayed vs τ for generic vacuum $U(1)$ symmetric model simulations with 256^2 (nothing) and 512^2 (triangles) spatial grid points. (See Figure 2 for initial data.)

Figure 2. Oscillatory behavior at a typical spatial grid point. The potentials V_1 and V_2 and φ are shown vs τ for a simulation with 128^2 spatial grid points. The initial data are $\Lambda = \sin u \sin v$, $x = z = \cos u \cos v$, $\varphi = \omega = 0$, $p_\Lambda = 14\, e^\Lambda$, $r = 10 \cos u \cos v$, and $p_z = p_x = 0$. The Hamiltonian constraint is solved for p. The initial value of τ is 10.

Figure 3. Oscillatory behavior at a typical spatial grid point. The same initial data as in Figure 2 but with 256^2 spatial grid points.

Figure 4. Oscillatory behavior at a typical spatial grid point. The same initial data as in Figure 2 but with 512^2 spatial grid points.

Figure 5. Oscillatory behavior at a typical spatial grid point. The same as Figure 2 but with Case B initial data: $\Lambda = \sin u \sin v$, $x = z = \cos u \cos v$, $\varphi = \omega = 0$, $p_\Lambda = 4\, e^\Lambda$, $p = \cos u \cos v$, and $p_z = p_x = 0$. The Hamiltonian constraint is solved for r. The initial value of τ is 10.

Figure 6. Behavior of (a) Λ and z, (b) ω, and (c) x in the simulation of Figure 3.

Figure 7. Movie frames of $\log_{10} \mathcal{H}_V(u, v)$ at (from right to left and top to bottom) $\tau = 14.9$, 19.8, 24.7, 29.6, 34.5, 39.5, 44.4, 49.3, 54.2. The range of values is -30 (black) to 3 (white). The simulation of Figure 3 provided the data.

Figure 8. Movie frames of $\varphi(u, v)$ at the same values of τ as in Figure 7, taken from the same simulation. The range of value is -27 (black) to 3.8 (white) on a linear scale.

Figure 9. The influence of spatial resolution. The variable φ on the line $u = v$ for $u, v \in [0, \pi]$ (vertical axis) is shown for $\tau \in [10, 53.5]$ (horizontal axis). The simulations of Figures 2 (top), 3, and 4 (bottom) are shown. The gray scale is similar to that in Figure 8.

Figure 10. The variable φ is shown for the line $u = v$ for $u, v \in [0, \pi]$ at $\tau = 53.5$ for a simulation with 256^2 spatial grid points (broken line) and 512^2 spatial grid points. These are the same simulations as in Figures 3 and 4 respectively.

Figure 11. $\mathrm{Log}_{10} V_1$ (left) and $\log_{10} V_2$ (right) for the line $u = v$ for $u, v \in [0, 2\pi]$ (vertical axis) and $\tau \in [10, 59]$ (horizontal axis) are shown on the same scale. The simulation of Figure 3 is used.

Figure 12. The final time step of Figure 11 is shown for $\log_{10} V_1$ (broken line), $\log_{10} V_2$ (thick solid line), and φ (thin solid line). The horizontal axis is the line $u = v$ for $u, v \in [0, \pi]$

[1] R. Penrose, Riv. Nuov. Cim., **1**, 252 (1969).
[2] S.W. Hawking, Proc. Roy. Soc. Lond. A, **300**, 182 (1967).
[3] S.W. Hawking and R. Penrose, Proc. Roy. Soc. Lond. A, **314**, 529 (1970).
[4] S.W. Hawking and G.F.R. Ellis, *The Large Scale Structure of Space-Time*, (Cambridge University Press, Cambridge,1973).
[5] R.M. Wald, *General Relativity*, (University of Chicago Press, Chicago, 1984).
[6] V.A. Belinskii and I.M. Khalatnikov, Sov. Phys. JETP, **30**, 1174 (1969).
[7] V.A. Belinskii and I.M. Khalatnikov, Sov. Phys. JETP, **29**, 911–917 (1969)
[8] V.A. Belinskii and I.M. Khalatnikov, Sov. Phys. JETP, **32**, 169–172 (1971).
[9] V.A. Belinskii, E.M. Lifshitz, and I.M. Khalatnikov, Sov. Phys. Usp. **13**, 745 (1971).
[10] V.A. Belinski, I.M. Khalatnikov and E.M. Lifshitz, Adv. Phys., **31**, 639 (1982).
[11] C. W. Misner, Phys. Rev. Lett. **22**, 1071 (1969).
[12] E. Kasner, Trans. Am. Math. Soc., **27**, 155–162, (1925).
[13] D.F. Chernoff and J.D. Barrow, Phys. Rev. Lett., **50**, 134 (1983).
[14] J.D. Barrow and F. Tipler, Phys. Rep. **56**, 372 (1979).
[15] B. Grubišić,in *Proceedings of the Cornelius Lanczos Symposium*, edited by J.D. Brown, M.T. Chu, D.C. Ellison, and R.J. Plemmons, (SIAM, Philadelphia,1994).
[16] J.A. Isenberg and V. Moncrief, Ann. Phys. (N.Y.) **199**, 84 (1990).
[17] B. Grubišić and V. Moncrief, Phys. Rev. D **47**, 2371 (1993).
[18] B.K. Berger and V. Moncrief, Phys. Rev. D, **48**, 4676 (1993).
[19] D. Eardley, E. Liang, and R. Sachs, J. Math. Phys., **13**, 99 (1972).
[20] R.H. Gowdy, Phys. Rev. Lett., **27**, 826 (1971).
[21] B.K. Berger, Ann. Phys. (N.Y.), **83**, 458, (1974).
[22] B.K. Berger, P.T. Chruściel, J. Isenberg, and V. Moncrief, Ann. Phys. (N.Y.), **260**, 117 (1997).
[23] J. Isenberg and S. Kichenassamy, "Polarized T^2-symmetric vacuum spacetimes," preprint.
[24] B.K. Berger, and D. Garfinkle, Phys. Rev. D, **57**, 4767 (1998).
[25] S. Kichenassamy and A.D. Rendall, Class. Quantum Grav., **15**, 1339 (1998).
[26] M. Weaver, J. Isenberg, and B.K. Berger, Phys. Rev. Lett., **80**, 2980 (1998).
[27] Y. Fujiwara, H. Ishihara, and H. Kodama, Class. Quantum Grav., **10**, 859 (1993).
[28] V.G. LeBlanc, D. Kerr, and J. Wainwright, Class. Quantum Grav.,**12**, 513, (1995).
[29] B.K. Berger,Class. Quantum Grav., **13**, 1273, (1996).
[30] V. Moncrief, Ann. Phys. (N.Y.), **167**, 118, (1986).
[31] B. Grubišić and V. Moncrief, Phys. Rev. D **49**, 2792 (1994).
[32] B.K. Berger and V. Moncrief, Phys. Rev. D, to be published, gr-qc/9801078.
[33] M.W. Choptuik, Phys. Rev. D **44**, 3124 (1991).
[34] B.K. Berger, D. Garfinkle, and E. Strasser, *Class. Quantum Grav.*, **14**, L29 (1997).
[35] J.A. Fleck, J.R. Morris, and M.D. Feit, Appl. Phys. **10**, 129 (1976).
[36] V. Moncrief, Phys. Rev. D **28**, 2485 (1983).
[37] M. Suzuki, Phys. Lett. A **146**, 319 (1990).
[38] M. Suzuki, J. Math. Phys. **32**, 400 (1991).
[39] A.H. Norton, U. of New South Wales preprint, 1992 (unpublished).
[40] I.M. Khalatnikov, E.M. Lifshitz, K.M. Khanin, L.N. Shchur, and Ya.G. Sinai, J. Stat. Phys., **38**, 97 (1985).
[41] A.A. Kirillov, and A.A. Kochnev, JETP Lett., **46**, 435, (1987).

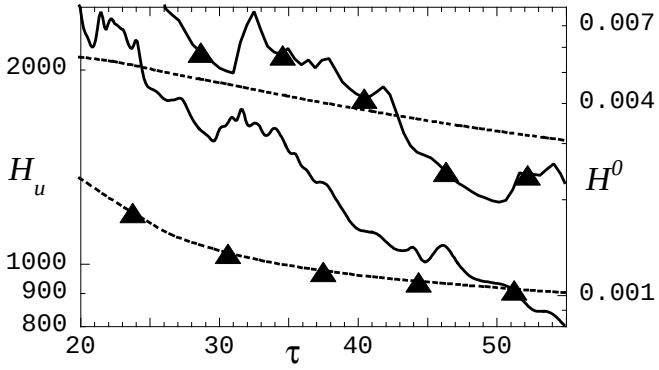

FIG. 1.

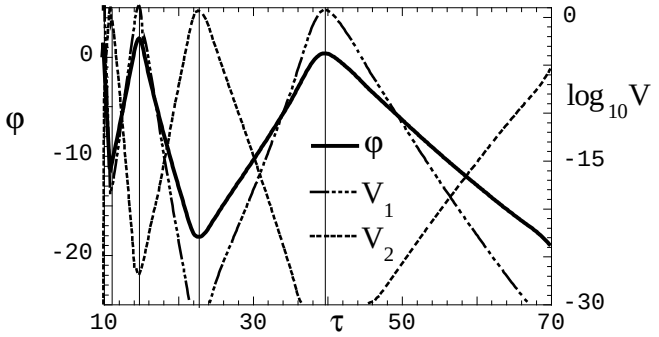

FIG. 2.

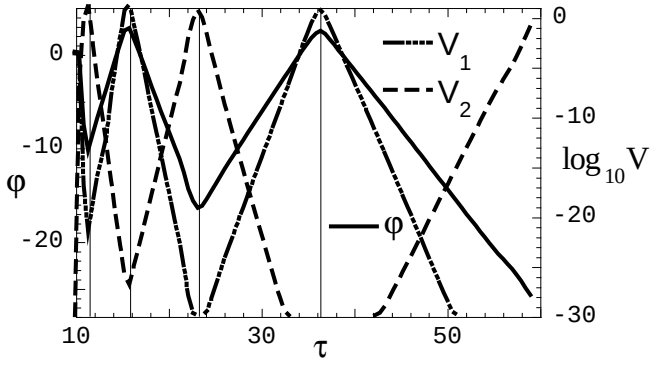

FIG. 3.

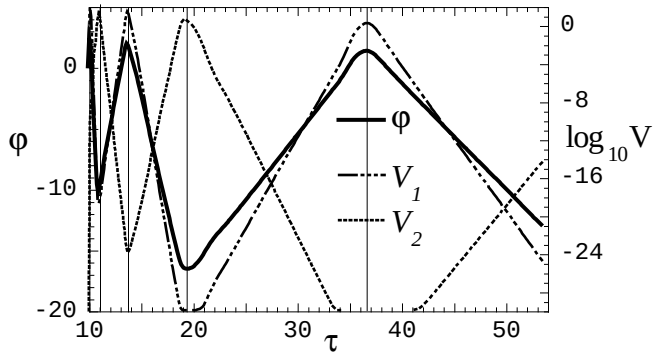
0
-10
-20
φ
10
20
30
40
50
τ
0
-8
-16
-24
log10V
φ
V1
V2

FIG. 4.

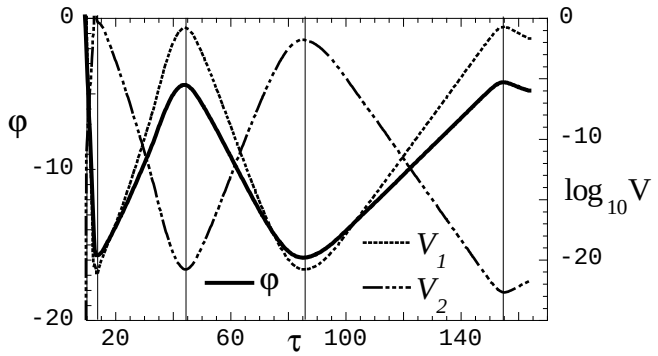
0
-10
-20
φ
20
60
100
140
τ
0
-10
-20
log10V
V1
φ
V2

FIG. 5.

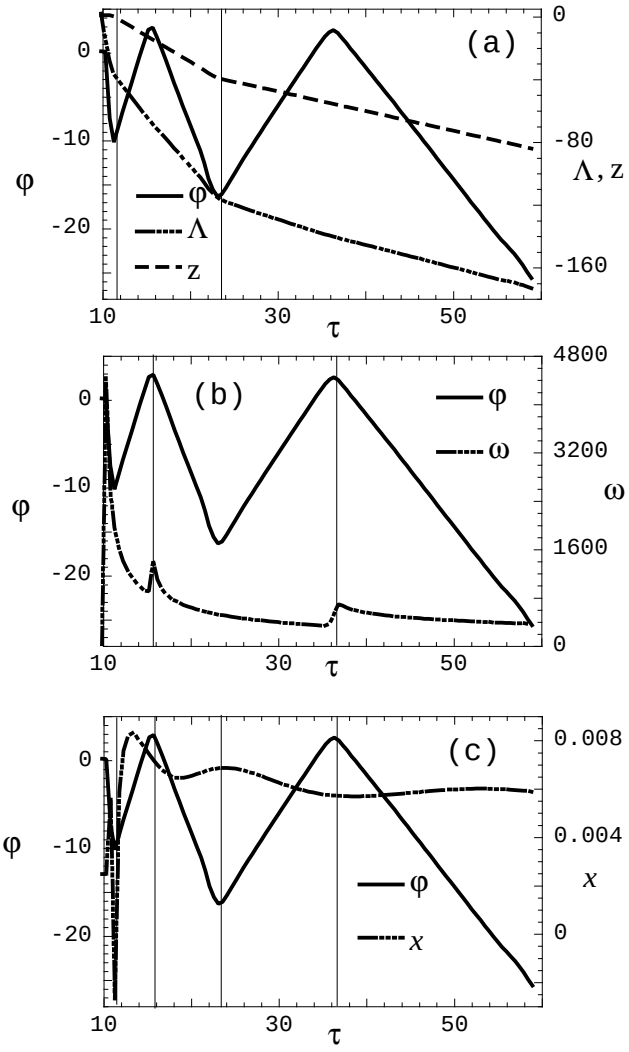

FIG. 6.

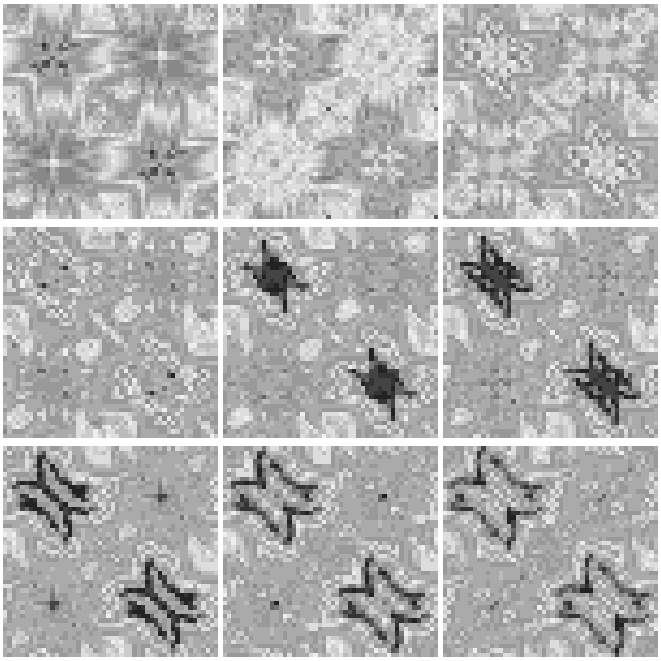

FIG. 7.

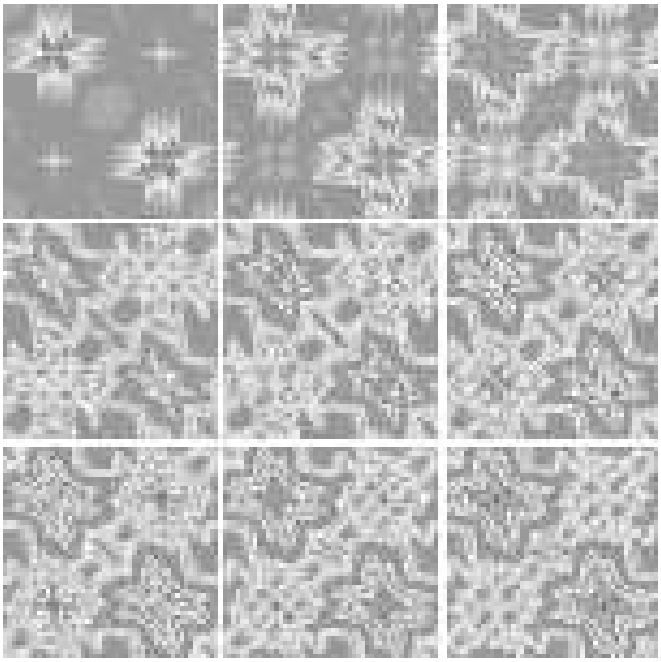

FIG. 8.

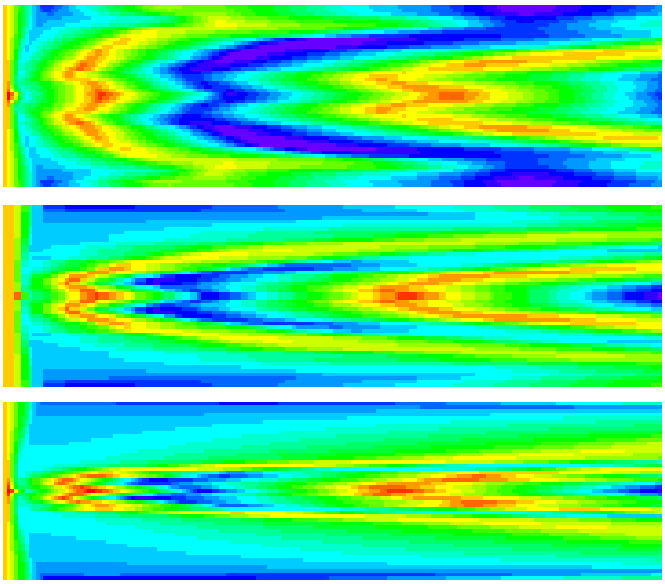

FIG. 9.

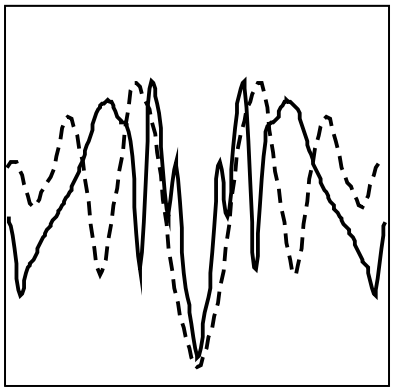

FIG. 10.

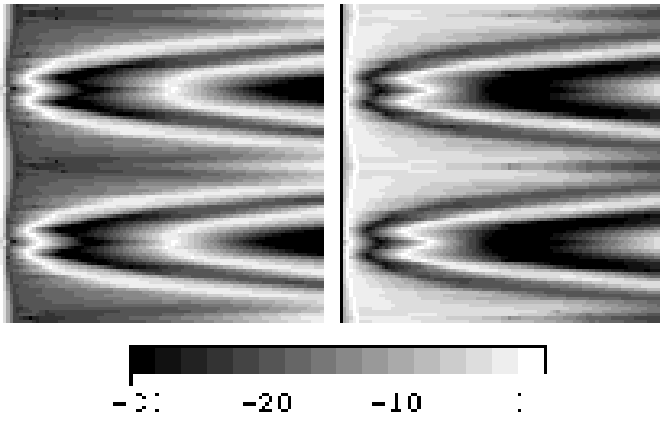

FIG. 11.

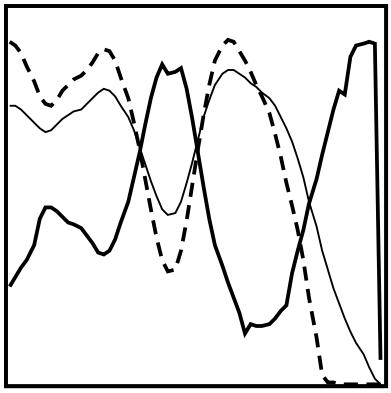

FIG. 12.